Atmos. Chem. Phys. Discuss., 13, 19895–19919, 2013
www.atmos-chem-phys-discuss.net/13/19895/2013/
doi:10.5194/acpd-13-19895-2013

Atmospheric Chemistry and Physics Discussions
Open Access

Longitudinal hot-spots in the mesospheric OH variations due to energetic electron precipitation

M. E. Andersson [1], P. T. Verronen [1], C. J. Rodger [2], M. A. Clilverd [3], and S. Wang [4]

[1]Earth Observation, Finnish Meteorological Institute, Helsinki, Finland
[2]Department of Physics, University of Otago, Dunedin, New Zealand
[3]British Antarctic Survey (NERC), Cambridge, UK
[4]Jet Propulsion Laboratory, California Institute of Technology, California, USA

Received: 13 June 2013 – Accepted: 18 July 2013 – Published: 26 July 2013

Correspondence to: M. E. Andersson (monika.andersson@fmi.fi)

Published by Copernicus Publications on behalf of the European Geosciences Union.

Abstract

Using Microwave Limb Sounder (MLS/Aura) and Medium Energy Proton and Electron Detector (MEPED/POES) observations between 2005–2009, we study the longitudinal response of nighttime mesospheric OH to radiation belt electron precipitation. Our analysis concentrates on geomagnetic latitudes from 55–72° N/S and altitudes between 70–78 km. The aim of this study is to better assess the spatial distribution of electron forcing, which is important for more accurate modeling of its atmospheric and climate effects. In the Southern Hemisphere, OH data show a hot-spot at longitudes between 150° W–30° E, i.e., poleward of the Southern Atlantic Magnetic Anomaly (SAMA) region. In the Northern Hemisphere, energetic electron precipitation–induced OH variations are more equally distributed with longitude. This longitudinal behaviour of OH can also be identified using Empirical Orthogonal Function analysis, and is found to be similar to that of MEPED–measured electron fluxes. The main difference is in the SAMA region, where MEPED appears to measure very large electron fluxes while MLS observations show no enhancement of OH. This indicates that in the SAMA region the MEPED observations are not related to precipitating electrons, at least not at energies > 100 keV, but related to instrument contamination. Analysis of selected OH data sets for periods of different geomagnetic activity levels shows that the longitudinal OH hot-spot south of the SAMA (the Antarctic Peninsula region) is partly caused by strong, regional electron forcing, although atmospheric conditions also seem to play a role. This OH hot-spot is even seen weakly during periods of lower geomagnetic activity, which suggest that there is a steady drizzle of electrons affecting the atmosphere, due to the Earth's magnetic field being weaker in this region.

1 Introduction

An important source of variability of mesospheric OH comes from energetic particle precipitation events that originate from explosions on the surface of the Sun (Thorne, 1977; Heaps, 1978; Verronen et al., 2006, 2007, 2011; Damiani et al., 2008, 2010b; Jackman et al., 2011). In contrast to solar protons, which propagate directly from the Sun into Earth's atmosphere, energetic electrons are first stored and energized in the radiation belts. During geomagnetic storms, strong acceleration and loss process occur (Reeves et al., 2003), which can both boost the trapped population and lead to significant loss of electrons into the atmosphere. Energetic electron precipitation (EEP) from the radiation belts affects the neutral atmosphere at magnetic latitudes of about 55–72° and results in the enhancement of HO_x through water cluster ion chemistry. This process is only effective below about 80 km, where enough water vapor is available (Solomon et al., 1981; Verronen and Lehmann, 2013). The atmospheric penetration depth depends on the energy of the particle, e.g. electrons with 100 keV and 3 MeV energy can reach 80 km and 50 km, respectively (see e.g. Turunen et al., 2009, Fig. 3).

The primary driver of the radiation belt variability is geomagnetic activity, which can come either from the coronal mass ejections (CMEs) during solar maximum or the high-speed solar wind-streams (HSSWS, $> 500\,\mathrm{km\,s^{-1}}$) which are most common during the declining and minimum phase of solar activity. The energy input to the magnetosphere during HSSWS events is comparable to or can be higher than the energy input during CMEs (Richardson et al., 2000, 2001).

EEP can occur on different timescales with varying significance for the atmospheric chemistry but our understanding of the nature of the precipitation as well as the variation of the electron flux lost to the atmosphere is limited. This is mostly due to spatial and temporal limitation of the measurements as well as contamination issues in the space–based instrumentation (Rodger et al., 2010a; Clilverd et al., 2010). Therefore, detailed study of the EEP effects in the atmosphere can significantly improve our understanding of the EEP variability which is important for atmospheric modeling (Funke et al., 2011).

Recent studies provided evidence of the connection between precipitating radiation belt electrons and mesospheric hydroxyl (Andersson et al., 2012; Verronen et al., 2011). By analyzing zonal mean time series of MLS/Aura OH mixing ratios

ACPD
13, 19895–19919, 2013

and MEPED/POES radiation belt electron fluxes during the period August 2004–December 2009, they demonstrated strong correlation between experimentally observed 100–300 keV electron count rates and nighttime OH concentrations below 80 km. These studies provided a lower-limit estimation of the importance of energetic electron precipitation on HO_x, showing that for the considered time period, EEP has measurable effects in about 30 % of cases.

In this paper, we combine MLS OH and MEPED EEP satellite measurements to study the longitudinal OH variations caused by precipitating radiation belt electrons between January 2005–December 2009. We go on to utilize empirical orthogonal function (EOF) analysis to identify OH spatial and temporal patterns of variability. Finally we provide clear evidence that the SAMA region influences the longitudinal variation of OH at geomagnetic latitudes 55–72° in the Southern Hemisphere (SH), as expected from the location of the radiation belts and the weaker magnetic field region.

2 Data

2.1 MLS/Aura observations

The MLS instrument onboard NASA's Aura satellite, placed into a Sun-synchronous orbit (about 705 km), samples up to 82° N/S (Waters et al., 2006). MLS observes thermal microwave emission, scanning from the ground to 90 km every 25 s with daily global coverage of about 13 orbits per day.

In this study, we use Version 3.3 Level 2 nighttime (solar zenith angle > 100°) OH for the time period of January 2005–December 2009 between 70–78 km altitude (corresponding to pressure levels between 0.046 and 0.015 hPa). The altitude selection was based on previous studies, i.e., (Andersson et al., 2012), which showed that between 70–78 km the response of OH to electron precipitation is the highest. The vertical resolution of OH observations is about 2.5 km and the systematic error is typically less than 10 %. The data were screened according to the MLS data description and quality

ACPD
13, 19895–19919, 2013

document (Livesey et al., 2011). The OH observations taken during solar proton events (SPE), which dominate the ionization in the middle atmosphere, were excluded here and from all further considerations using a flux limit of 4 protons $cm^{-2} s^{-1} sr^{-1}$ observed by GOES-11 in 5–10 MeV channel.

In addition, to support our discussion about OH variations, we also use MLS water vapor (H_2O) and temperature observations. The H_2O and temperature data were sampled the same way as the OH measurements and screened according to the MLS data quality document. The vertical resolution of H_2O/temperature observations is coarser than that of OH at considered altitudes, i.e., about 5 km, and therefore, we use measurements between 70–76 km (corresponding to pressure levels between 0.046 and 0.025 hPa). The systematic error of the H_2O/temperature data is typically less than 25 %/5 %. Details on the validation of the MLS OH, H_2O and temperature are given in Pickett et al. (2008); Lambert et al. (2007) and Schwartz et al. (2008), respectively. Note, that due to the selection criteria we have more observations during the winter time.

3 MEPED/POES observation

The Space Environment Monitor (SEM-2) instrument package onboard the Sun-synchronous (800–850 km) NOAA POES satellites, provides long-term global measurement of precipitating electron fluxes with some limited energy spectra information. SEM-2 includes the Medium Energy Proton and Electron Detector (MEPED) which consists of two electron telescopes and two proton telescopes pointed approximately perpendicular to each other. Both electron telescopes provide three channels of energetic electron data: > 30 keV, > 100 keV, and > 300 keV, sampled simultaneously. For a detailed description of the SEM-2 instruments, see Evans and Greer (2004).

We utilize data from the MEPED 0° electron telescope (field of view is outward along the local zenith, parallel to the Earth-center-to-satellite radial vector). The electron telescopes are observing fluxes located inside the bounce loss cone, and thus electrons

ACPD
13, 19895–19919, 2013

which are being lost locally toward the spacecraft direction (Rodger et al., 2010a,b). At this point NOAA is undertaking major new data re-processing, which will produce new datasets with derived uncertainty values. Until these have been produced we suggest a reasonable value for the measurement uncertainties is 20 %, following Tan et al. (2007).

4 Results

Figure 1 shows the distribution of > 30 keV electrons precipitating into the atmosphere observed by the 0° directed MEPED-telescopes in 2005, 2006, 2008 and 2009. These maps were produced from the 2 s resolution electron telescope data, which were corrected for proton contamination (Yando et al., 2011) using the algorithm described in Appendix A of Lam et al. (2010). For each day of the year selected, a 1° spatial resolution map of the median > 30 keV fluxes was produced for each POES spacecraft in subsatellite coordinates. The median of each of these daily maps produces the median world maps shown in Fig. 1. While the Lam et al. (2010) method can generally correct for proton contamination, this is not possible when the electron observations are dominated by proton counts, as expected in SPE or in the SAMA region. The data inside the SAMA region, i.e., around 30° E–90° W and 0–45° S, appears to contain an increased particle background due to a local minimum of the geomagnetic field. In Fig. 1 the electron precipitation is confined to the geomagnetic latitudinal bands 55–72° N and 55–72° S and can occur at all geographic longitudes. However, in the SH the observed electron fluxes are consistently higher poleward of the SAMA region, i.e., the Antarctic Penisula (AP) hot-spot, which ranges in longitudinal extent from 180° W–60° E. There is less electron precipitation at longitudes between 90–180° E. The maximum difference in longitudinal EEP distribution within the range of the radiation belt in the SH is of about 150 %. In the Northern Hemisphere (NH) precipitation is more homogenous through the whole longitude range with lower electron fluxes observed between 150–30° W, i.e., North America (NAm) hot-spot. The maximum difference in longitudinal EEP distribution within the range of the radiation belt in the NH is of about 70 %. A similar geographic distribution of the precipitating electrons is observed for all considered years, with a decreasing trend of electron fluxes in the radiation belts from 2005 to 2009, related to the decline in solar activity. As noted above, Fig. 1 shows a clear pattern with a local hot-spot in precipitating fluxes in the AP region. This is expected, due to the changing strength of the geomagnatic field. In this region the magnetic field is weaker, such that the angular width of the bounce loss cone increases and electrons which were mirroring just above the atmosphere at other longitudes will be lost inside the atmosphere in this longitude region. The hot-spot is produced by the latitude range of the radiation belts, and by the increased bounce loss cone width caused by the local minima in magnetic field strength.

To contrast Fig. 1 and hence produce a typical representation of the longitudinal OH variations caused by electron precipitation, we calculated yearly medians from night-time OH averaged daily between 70–78 km. The results for 2005, 2006, 2008 and 2009 are presented in Fig. 2. At the geomagnetic latitudes affected by radiation belt electron precipitation in Fig. 1, i.e., 55–72°, OH medians are 20–50 % and 30–60 % higher in the NH and SH, respectively, than those at other geographic locations. The geographic distribution of the OH high values in both hemispheres is very similar to the distribution of precipitating electrons, i.e., OH follows geomagnetic rather than geographic latitudes. In the SH, the maximum values of OH are confined to the longitudinal range between 180° W–30° E (AP hot-spot). Similarly in the NH, the highest OH values are confined to the longitudes from 180° W–30° E (NAm hot-spot). The maximum difference in longitudinal OH distribution within the range of the radiation belt is of about 30/60 % in the NH and SH, respectively. The OH decrease between 2005–2009 clearly shows that the changes in OH are consistent with declining solar and geomagnetic activity. In the SAMA region itself, due to data contamination produced by inner radiation belt protons we observe no enhancement in OH. This indicates that in the SAMA region there is no significant > 100 keV electron precipitation, even though precipitating fluxes generally appear to peak in this region. This is consistent with our suggestion that the signal

ACPD
13, 19895–19919, 2013

above South America is due to data contamination, and in reality little precipitation is taking place, consistent with the very low geomagnetic latitudes relative to the locations of the inner and outer radiation belts. At the geomagnetic latitudes affected by electron precipitation, the mesospheric OH shows clear hemispheric asymmetry. The OH abundance in the SH is roughly twice that of the NH values for all the years considered. The reason for this behaviour is mainly due to differences in local solar time (LST) of the Aura satellite observations at the radiation belt latitudes. MLS measurements in the NH occur between 02.15–3.30 a.m. whereas in the SH the measurements occur around midnight, i.e., between 23.30–1.15.

In order to quantitatively assess the role of LST in hemispheric discrepancies, we used the Sodankylä Ion and Neutral Chemistry model (SIC). SIC is a 1-D model of the middle atmosphere and includes a standard set of HO_x chemistry. A detailed description of the model is available in the literature (Verronen et al., 2005; Verronen, 2006; Turunen et al., 2009). The model run was made for the 5–6 March 2005 and 12–13 April 2006 at 60° N/65° S and 0° E, using MLS/Aura monthly mean values of H_2O and temperature. Note, that no electron forcing was applied to the model in order to get the general behaviour of the OH during nighttime. Figure 3 gives an example of the OH mixing ratios from SIC model run averaged between 70–78 km. The modeled OH mixing ratios at LST of the satellite passage (gray areas) are of about 30–40 % higher in the SH than those in the NH. In general, OH is expected to decrease from sunset to sunrise but the magnitude of NH–SH differences can vary from month to month (i.e., March is different from April) because of atmospheric conditions. The model results suggest that LST plays a significant part in the OH hemispheric asymmetry. Note that, in addition to the LST, different atmospheric in-situ conditions e.g., amount of H_2O and temperature can also contribute to the hemispheric differences. Also, solar zenith angle (SZA) differences, on average 5–10° between NH–NAm and SH–AP hot-spots, could account for about 10–15 % of OH differences (see Minschwaner et al., 2011).

In order to analyze the EEP-induced longitudinal OH variations in detail, we calculated spatial distributions of nighttime OH medians between 70–78 km and 2005–

ACPD
13, 19895–19919, 2013

2009 for two selected data sets, different in the strength of EEP forcing. The data sets were: (1) high energetic electron precipitation (HEEP) set, i.e., daily mean electron count rates (ECR) measured by MEPED $> 100\,\mathrm{counts\,s^{-1}}$, 51 days of data in total; (2) low energetic electron precipitation (LEEP) set, ECR $< 5\,\mathrm{counts\,s^{-1}}$, 1340 days in total. Contrasting these two data sets allows us to see what proportion of the longitudinal OH-hot-spots is caused by EEP. The results are presented in Fig. 4. During the LEEP period, high OH values are centered around the geographic pole with maximum OH inside the radiation belt in the AP sector (bottom right panel), while in the NH there is slightly more OH over the NAm sector compared to other longitudes (top right panel). The enhanced values in the SH in the AP sector could be connected to the steady drizzle of radiation belt electrons continuously affecting the mesosphere even during LEEP conditions (Clilverd et al., 2010b), as well as different atmospheric conditions (discussed in the next paragraph). During the HEEP periods, SH–OH longitudinal structure is preserved, i.e., OH clearly peaks in the AP sector. In the NH, OH enhancements due to EEP are more equally distributed between 90° W–90° E, i.e., NAm and North Asia (NAs) sectors.

Because the differences in H_2O and temperature could cause some of the observed OH longitudinal variability in Fig. 4, we examine their possible role in the observed OH enhancements in the AP sector. Figure 5 shows H_2O (left panel) and temperature (right panel) medians calculated for the LEEP data set, i.e., daily mean ECR $< 5\,\mathrm{counts\,s^{-1}}$. Before calculating the median values, nightime mean H_2O and temperature measurements were averaged between 70–76 km. In the SH, low H_2O and high temperature values are centered around the geographic pole. In the radiation belt latitudes, low H_2O corresponds to the high OH values (see bottom right panel of the Fig. 4) and therefore the H_2O can not explain the OH enhancement in the AP region. Because temperature and OH are positively correlated at altitudes below 80 km (Damiani et al., 2010a), OH enhancement in the AP sector can be partially explained by the higher temperature observed in this region. In order to quantify the sensitivity of OH to the temperature during LEEP and separate them from EEP-induced OH enhancements, we again used the

SIC model. All model runs were made between 5 (12:00 UT)–6 (12:00 UT) March 2005 at 60° N/65° S and 0° E with high electron-precipitation produced ionization rates, i.e., 1000 $cm^{-3} s^{-1}$. First, we made model runs using MLS monthly mean values of the temperature, i.e., 100 %T. Then we changed the temperature according to the longitudinal variability observed during LEEP, i.e., 110 %T (see Fig. 5). The obtained results (not shown here) indicate that increasing temperature by 10 % (similar to that seen in the region around the AP region) increases nighttime OH mixing ratio in average by about 15–25 %. In addition, the average difference between longitudinal distribution of SZA of about 20°, can account for about 25–30 % of longitudinal variability. Therefore, the stronger OH response in the AP sector (80 % higher than at the other longitudes) can not be explained only by different atmospheric conditions but is most likely also connected to the peak in electron precipitation forcing seen to occur in the same spatial region.

Summarizing our analysis, Fig. 6 shows the radiation belt OH medians for 4 data sets: (I) days (30 for NH, 40 for SH) between 2005–2009 with ECR > 100 counts s^{-1} (high precipitation, again termed HEEP), (II) days (723 for NH, 767 for SH) between 2005–2009 with ECR < 5 counts s^{-1} (low precipitation, termed LEEP), (III) days (264 for NH, 267 for SH) between 2005–2006 with ECR < 5 counts s^{-1}, (low precipitation, high geomagnetic activity years), (IV) days (141 for NH, 163 for SH) in 2009 with ECR < 5 counts s^{-1} (low precipitation, low geomagnetic activity years). Note, that only days with full longitudinal coverage were taken into account, which basically excludes the summer time periods. In addition to the HEEP (I) and LEEP (II) which we already considered when discussing Fig. 4, cases III and IV are needed to investigate possible influences from the steady drizzle of radiation belt electrons continuously affecting the mesosphere even during LEEP conditions. For all considered cases (I–IV), SH–OH shows stronger longitudinal variability, which is primarily caused by geomagnetic latitude selection, and therefore, different atmospheric conditions (H_2O, temperature and SZA). The absolute/relative OH differences between case I and IV are of about the same magnitude in the NH and SH, varying from 0.04–0.46 ppbv/0–60 %. The maximum OH enhancements in the NH are more equally distributed, i.e., confined to the longitudinal range between 90° E–90° W. In the SH, the largest increase is seen in the AP sector i.e., 180° W–0° E which is likely to be connected to the stronger EEP forcing in this region. Comparison between case III and IV shows that in the SH, in the AP region, OH values are about 5–20 % higher during the periods selected by case III. This again may indicate steady drizzle of radiation belt electrons in the SH, around the AP even during geomagnetically quiet time conditions. In the NH, OH mean values during the periods selected by cases III and IV are comparable.

Finally, to test our results with a completely different method, Empirical Orthogonal Function (EOF) analysis has been performed. The EOF method decomposes the data set into a set of orthogonal basis functions in order to find the structures (EOF modes) that explain the maximum amount of variance in a two dimensional data set as well as their time variations, i.e., Principal Components (PC). More details about can be found in van Storch and Zwiers (1999, and references therein). The EOF analysis was conducted for 6 selected months between 2005–2009. i.e. March–April 2005, September 2005, March–April 2006 and March 2008. The months were selected for 2 reasons: (1) high EEP events were observed for each month; (2) full global coverage during spring/autumn periods in both hemispheres with similar numbers of profiles selected and similar in-situ atmospheric conditions. The nighttime OH data were divided into 5 (latitude) ×30 (longitude) degree bins. The OH monthly mean was removed, leaving anomalies that retain variation on daily to inter-annual time scales. The leading EOF spatial pattern and EOF time series were calculated for the anomaly fields averaged between 70–78 km. Both, EOF and PC were normalized and the physical units follow normal convention of presenting EOFs. The results of EOF analysis, i.e., first EOF along with the variance explained (%) and corresponding PC 1, are shown in Fig. 7. Figure 7 also shows the median distribution of > 30 keV electrons precipitating into the atmosphere observed by the 0° directed MEPED for the same months EOF analysis was conducted.

ACPD
13, 19895–19919, 2013

The observed electron precipitation seen in the upper left hand panel of this figure is similar to the yearly medians presented in Fig. 1 except that is has a more pronounced longitudinal structure. EEP is clearly higher in the AP region and slightly higher between 150° E–0° W in the NH in the magnetic latitudinal band 55–72° N/S. The first EOF (right top panel of the Fig. 7) also has pronounced structures at geomagnetic latitudes connected to the radiation belts (55–72° N/S) and appears to be associated with the spatial variations in the precipitating electrons. The spatial patterns of the OH changes do not extend to the other latitudes. EOF 1 constitutes 6 % of the total variance, and this mode clearly dominates the OH variation after a strong global seasonal component was removed. The Principal component (PC 1) related to the first EOF follows the ECR variability (bottom panel of Fig. 7). The amplitude of the PC 1 is highly correlated with ECR, with $r_{\mathrm{EOF}} = 0.6$ and $p = 0$ (t test). These results indicate that first EOF is associated with EEP. EOF 1 not only reflects an enhancement of OH at latitudes affected by EEP but also captures its longitudinal variations, i.e., maximum increases confined to the longitudinal band 150° E–30° W in the NH and 180° W–60° E in the SH (see Fig. 4). We analyzed also the second and third EOF patterns (not shown). However, these sum up to less than 3 % of the total variance and the patterns do not correlate with EEP. They are more likely connected to the noise.

5 Conclusions

Using measurements from the MLS/Aura and MEPED/POES between 2005–2009, we have studied longitudinal variations of nighttime OH and their link to energetic electron precipitation. Our analysis shows, that at geomagnetic latitudes 55–72° N/S and altitudes between 70–78 km, there are spatial hot-spots in the mesospheric OH variations due to energetic electron precipitation.

In the SH, an OH hot-spot is located in the AP region, i.e., in a longitudinal band between 150° W–60° E. At those longitudes, EEP observed by POES, as well as the OH enhancement are the highest. Because the atmospheric in-situ conditions can ex-

ACPD
13, 19895–19919, 2013

plain only part of the total 80 % of OH longitudinal variations (15–25 % H_2O and temperature, 25–30 % SZA), the OH hot-spot in this sector is likely to be connected to stronger electron forcing. Also, increased OH values in this region during the period of low EEP but higher geomagnetic activity suggest the effect of a steady drizzle of radiation belt electrons during the quiet time conditions. EOF analysis has shown similar pronounced structures at geomagnetic latitudes connected to the radiation belts (55–72° S). The first EOF mode constitutes 6 % of the total variance, and clearly reflects an enhancement of OH at latitudes affected by EEP as well as its longitudinal variations, i.e., a maximum amplitude confined to the longitudinal band 150° W–60° E. Note, that even though MEPED measures very high electron count rates inside SAMA, this does not seem to correspond to any significant precipitation, i.e., no OH enhancement is observed in that region.

In the NH, EEP is more homogenous over the whole longitude range with slightly higher electron fluxes observed between 180° W–0° E, i.e., over the NAm sector. The distribution of OH yearly medians is roughly confined to the same longitudinal band 150° W–30° E, but the OH medians during HEEP show different spatial behaviour, i.e., an OH hot-spot extends from NAm to the NAs sector (90° E–90° W). The first EOF mode clearly reflects the OH enhancement with the maximum amplitude roughly confined to the longitudinal band 150° W–30° E.

Our analysis has shown a significant role of the particle precipitation in the OH distribution at latitudes connected to the radiation belt, which is especially important in the SH due to the local weakness in the Earth's magnetic field. Taking into account the OH longitudinal variations due to the energetic electrons precipitation is important from the point of view of the atmospheric modelling in order to better represent polar regions.

Acknowledgements. The work of M. E. A. and P. T. V. was supported by the Academy of Finland through the projects #136225 and #140888 (SPOC: Significance of Energetic Electron Precipitation to Odd Hydrogen, Ozone, and Climate). CJR was supported by the New Zealand Marsden fund. S. W. was supported by the NASA Aura Science Team program.

ACPD
13, 19895–19919, 2013

References

Andersson, M. E., Verronen, P. T., Wang, S., Rodger, C. J., Clilverd, M. A., and Carson, B.: Precipitating radiation belt electrons and enhancements of mesospheric hydroxyl during 2004–2009, J. Geophys. Res., 117, D09304, doi:10.1029/2011JD017246, 2012. 19897, 19898

Clilverd, M. A., Rodger, C. J., Moffat-Griffin, T., Spanswick, E., Breen, P., Menk, F. W., Grew, R. S., Hayashi, K., and Mann, I. R.: Energetic outer radiation belt electron precipitation during recurrent solar activity, J. Geophys. Res., 115, A08323, doi:10.1029/2009JA015204, 2010a. 19897

Clilverd, M. A., Rodger, C. J., Gamble, R. J., Ulich, T., Raita, T., Seppälä, A., Green, J. C., Thomson, N. R., Sauvaud, J.-A., and Parrotet, M.: Ground-based estimates of outer radiation belt energetic electron precipitation fluxes into the atmosphere, J. Geophys. Res., 115, A12304, doi:10.1029/2010JA015638, 2010b. 19903

Damiani, A., Storini, M., Laurenza, M., and Rafanelli, C.: Solar particle effects on minor components of the Polar atmosphere, Ann. Geophys., 26, 361–370, doi:10.5194/angeo-26-361-2008, 2008. 19897

Damiani, A., Storini, M., Santee, M. L., and Wang, S.: Variability of the nighttime OH layer and mesospheric ozone at high latitudes during northern winter: influence of meteorology, Atmos. Chem. Phys., 10, 10291–10303, doi:10.5194/acp-10-10291-2010, 2010a. 19903

Damiani, A., Storini, M., Santee, M. L., and Wang, S.: The hydroxyl radical as an indicator of SEP fluxes in the high-latitude terrestrial atmosphere, Adv. Space Res., 46, 1225–1235, doi:10.1016/j.asr.2010.06.022, 2010b. 19897

Evans, D. S. and Greer, M. S.: Polar Orbiting environmental satellite space environment monitor – 2. instrument descriptions and archive data documentation, NOAA Technical Memorandum version 1.4, Space Environment Laboratory, Colorado, 2004. 19899

Funke, B., Baumgaertner, A., Calisto, M., Egorova, T., Jackman, C. H., Kieser, J., Krivolutsky, A., López-Puertas, M., Marsh, D. R., Reddmann, T., Rozanov, E., Salmi, S.-M., Sinnhuber, M., Stiller, G. P., Verronen, P. T., Versick, S., von Clarmann, T., Vyushkova, T. Y., Wieters, N., and Wissing, J. M.: Composition changes after the "Halloween" solar proton event: the High Energy Particle Precipitation in the Atmosphere (HEPPA) model versus MIPAS data intercomparison study, Atmos. Chem. Phys., 11, 9089–9139, doi:10.5194/acp-11-9089-2011, 2011. 19897

Heaps, M. G.: The effect of a solar proton event on the minor neutral constituents of the summer polar mesosphere, Tech. Rep. ASL-TR0012, US Army Atmos. Sci. Lab., White Sands Missile Range, NM, 1978. 19897

Jackman, C. H., Marsh, D. R., Vitt, F. M., Roble, R. G., Randall, C. E., Bernath, P. F., Funke, B., López-Puertas, M., Versick, S., Stiller, G. P., Tylka, A. J., and Fleming, E. L.: Northern Hemisphere atmospheric influence of the solar proton events and ground level enhancement in January 2005, Atmos. Chem. Phys., 11, 6153–6166, doi:10.5194/acp-11-6153-2011, 2011. 19897

Lam, M. M., Horne, R. B., Meredith, N. P., Glauert, S. A., Moffat-Griffin, T., and Green, J. C.: Origin of energetic electron precipitation >30 keV into the atmosphere, J. Geophys. Res., 115, A00F08, doi:10.1029/2009JA014619, 2010. 19900

Lambert, A., Read, W. G., Livesey, N. J., Santee, M. L., Manney, G. L., Froidevaux, L., Wu, D. L., Schwartz, M. J., Pumphrey, H. C., Jimenez, C., Nedoluha, G. E., Cofield, R. E., Cuddy, D. T., Daffer, W. H., Drouin, B. J., Fuller, R. A., Jarnot, R. F., Knosp, B. W., Pickett, H. M., Perun, V. S., Snyder, W. V., Stek, P. C., Thurstans, R. P., Wagner, P. A., Waters, J. W., Jucks, K. W., Toon, G. C., Stachnik, R. A., Bernath, P. F., Boone, C. D., Walker, K. A., Urban, J., Murtagh, D., Elkins, J. W., and Atlas, E.: Validation of the Aura Microwave Limb Sounder middle atmosphere water vapor and nitrous oxide measurements, J. Geophys. Res., 112, D24S32, doi:10.1029/2007JD008724, 2007. 19899

Livesey, N. J., Read, W. G., Froidevaux, L., Lambert, A., Manney, G. L., Pumphrey, H. C., Santee, M. L., Schwartz, M. J., Wang, S., Cofield, R. E., Cuddy, D. T., Fuller, R. A., Jarnot, R. F., Jiang, J. H., Knosp, B. W., Stek, P. C., Wagner, P. A., and Wu, D. L.: EOS MLS Version 3.3 Level 2 data quality and description document, JPL D-33509, Jet Propulsion Laboratory, Version 3.3x-1.0, 18 January, 2011. 19899

Minschwaner, K., Manney, G. L., Wang, S. H., and Harwood, R. S.: Hydroxyl in the stratosphere and mesosphere – Part 1: Diurnal variability, Atmos. Chem. Phys., 11, 955–962, doi:10.5194/acp-11-955-2011, 2011. 19902

Pickett, H. M., Drouin, B. J., Canty, T., Salawitch, R. J., Fuller, R. A., Perun, V. S., Livesey, N. J., Waters, J. W., Stachnik, R. A., Sander, S. P., Traub, W. A., Jucks, K. W., and Minschwaner, K.: Validation of aura microwave limb sounder OH and HO_2 measurements, J. Geophys. Res., 113, D16S30, doi:10.1029/2007JD008775, 2008. 19899

Reeves, G. D., McAdams, K. L., Friedel, R. H. W., and O'Brien, T. P.: Acceleration and loss of relativistic electrons during geomagnetic storms, Geophys. Res. Lett., 30, 1529, doi:10.1029/2002GL016513, 2003. 19897

Richardson, I. G., Cliver, E. W., and Cane, H. V.; Sources of geomagnetic activity over the solar cycle: relative importance of coronal mass ejections, high-speed streams, and slow solar wind, J. Geophys. Res., 105, 18203–18213, 2000. 19897

Richardson, I. G., Cliver, E. W., and Cane, H. V.: Sources of geomagnetic storms for solar minimum and maximum conditions during 1972–2000, Geophys. Res. Lett., 28, 2569–2572, 2001. 19897

Rodger, C. J., Clilverd, M. A., Green, J. C., and Lam, M. M.: Use of POES SEM-2 observations to examine radiation belt dynamics and energetic electron precipitation into the atmosphere, J. Geophys. Res., 115, A04202, doi:10.1029/2008JA014023, 2010a. 19897, 19900

Rodger, C. J., Carson, B. R., Cummer, S. A., Gamble, R. J., Clilverd, M. A., Sauvaud, J.-A., Parrot, M., Green, J. C., and Berthelier, J.-J.: Contrasting the efficiency of radiation belt losses caused by ducted and non-ducted whistler mode waves from ground-based transmitters, J. Geophys. Res., 115, A12208, doi:10.1029/2010JA015880, 2010b. 19900

Schwartz, M. J., Lambert, A., Manney, G. L., Read, W. G., Livesey, N. J., Froidevaux, L., Ao, C. O., Bernath, P. F., Boone, C. D., Cofield, R. E., Daffer, W. H., Drouin, B. J., Fetzer, E. J., Fuller, R. A., Jarnot, R. F., Jiang, J. H., Jiang, Y. B., Knosp, B. W., Krüger, K., Li, J.-L. F., Mlynczak, M. G., Pawson, S., Russell III, J. M., Santee, M. L., Snyder, W. V., Stek, P. C., Thurstans, R. P., Tompkins, A. M., Wagner, P. A., Walker, K. A., Waters, J. W., and Wu, D. L.: Validation of the aura microwave limb sounder temperature and geopotential height measurements, J. Geophys. Res., 113, D15S11, doi:10.1029/2007JD008783, 2008. 19899

Solomon, S., Rusch, D. W., Gérard, J.-C., Reid, G. C., and Crutzen, P. J.: The effect of particle precipitation events on the neutral and ion chemistry of the middle atmosphere: II. Odd hydrogen, Planet. Space Sci., 8, 885–893, 1981. 19897

Tan, L. C., Fung, S. F., and Shao, X.: NOAA/POES MEPED Data Documentation: NOAA-5 to NOAA-14 Data Reprocessed at GSFC/SPDF, NASA, Space Physics Data Facility, 2007. 19900

Thorne, R. M.: Energetic radiation belt electron precipitation – a natural depletion mechanism for stratospheric ozone, Science, 195, 287–289, 1977. 19896

Turunen, E., Verronen, P. T., Seppälä, A., Rodger, C. J., Clilverd, M. A., Tamminen, J., Enell, C.-F., and Ulich, T.: Impact of different precipitation energies on NO_x generation during geomagnetic storms, J. Atmos. Sol.-Terr. Phys., 71, 1176–1189, doi:10.1016/j.jastp.2008.07.005, 2009. 19897, 19902

van Storch, H. and Zwiers, F. W.: Statistical Analysis in Climate Research, Cambridge University Press, New York, 1999. 19905

Verronen, P. T.: Ionosphere–atmosphere interaction during solar proton events, no. 55, Finnish Meteorological Institute Contributions, Finnish Meteorological Institute, Helsinki, Finland, available at: http://urn.fi/URN:ISBN:952-10-3111-5, 2006. 19902

Verronen, P. T. and Lehmann, R.: Analysis and parameterisation of ionic reactions affecting middle atmospheric HO_x and NO_y during solar proton events, Ann. Geophys., 31, 909–956, doi:10.5194/angeo-31-909-2013, 2013. 19897

Verronen, P. T., Seppälä, A., Clilverd, M. A., Rodger, C. J., Kyrölä, E., Enell, C.-F., Ulich, T., and Turunen, E.: Diurnal variation of ozone depletion during the October–November 2003 solar proton events, J. Geophys. Res., 110, A09S32, doi:10.1029/2004JA010932, 2005. 19902

Verronen, P. T., Seppälä, A., Kyrölä, E., Tamminen, J., Pickett, H. M., and Turunen, E.: Production of odd hydrogen in the mesosphere during the January 2005 solar proton event, Geophys. Res. Lett., 33, L24811, doi:10.1029/2006GL028115, 2006. 19897

Verronen, P. T., Rodger, C. J., Clilverd, M. A., Pickett, H. M., and Turunen, E.: Latitudinal extent of the January 2005 solar proton event in the Northern Hemisphere from satellite observations of hydroxyl, Ann. Geophys., 25, 2203–2215, doi:10.5194/angeo-25-2203-2007, 2007. 19897

Verronen, P. T., Rodger, C. J., Clilverd, M. A., and Wang, S.: First evidence of mesospheric hydroxyl response to electron precipitation from the radiation belts, J. Geophys. Res., 116, D07307, doi:10.1029/2010JD014965, 2011. 19897

Waters, J. W., Froidevaux, L., Harwood, R. S., Jarnot, R. F., Pickett, H. M., Read, W. G., Siegel, P. H., Cofield, R. E., Filipiak, M. J., Flower, D. A., Holden, J. R., Lau, G. K., Livesey, N. J., Manney, G. L., Pumphrey, H. C., Santee, M. L., Wu, D. L., Cuddy, D. T., Lay, R. R., Loo, M. S., Perun, V. S., Schwartz, M. J., Stek, P. C., Thurstans, R. P., Boyles, M. A., Chandra, K. M., Chavez, M. C., Chen, G.-S., Chudasama, B. V., Dodge, R., Fuller, R. A., Girard, M. A., Jiang, J. H., Jiang, Y., Knosp, B. W., Labelle, R. C., Lam, J. C., Lee, A. K., Miller, D., Oswald, J. E., Patel, N. C., Pukala, D. M., Quintero, O., Scaff, D. M., Vansnyder, W., Tope, M. C., Wagner, P. A., and Walch, M. J.: The Earth Observing System

ACPD
13, 19895–19919, 2013

Microwave Limb Sounder (EOS MLS) on the Aura satellite, IEEE T. Geosci. Remote, 44, 1075–1092, doi:10.1109/TGRS.2006.873771, 2006. 19898

Yando, K., Millan, R. M., Green, J. C., and Evans, D. S.: A Monte Carlo simulation of the NOAA POES medium energy proton and electron detector instrument, J. Geophys. Res., 116, A10231, doi:10.1029/2011JA016671, 2011. 19900

ACPD

13, 19895–19919, 2013

Electron precipitation and spatial OH variations

M. E. Andersson et al.

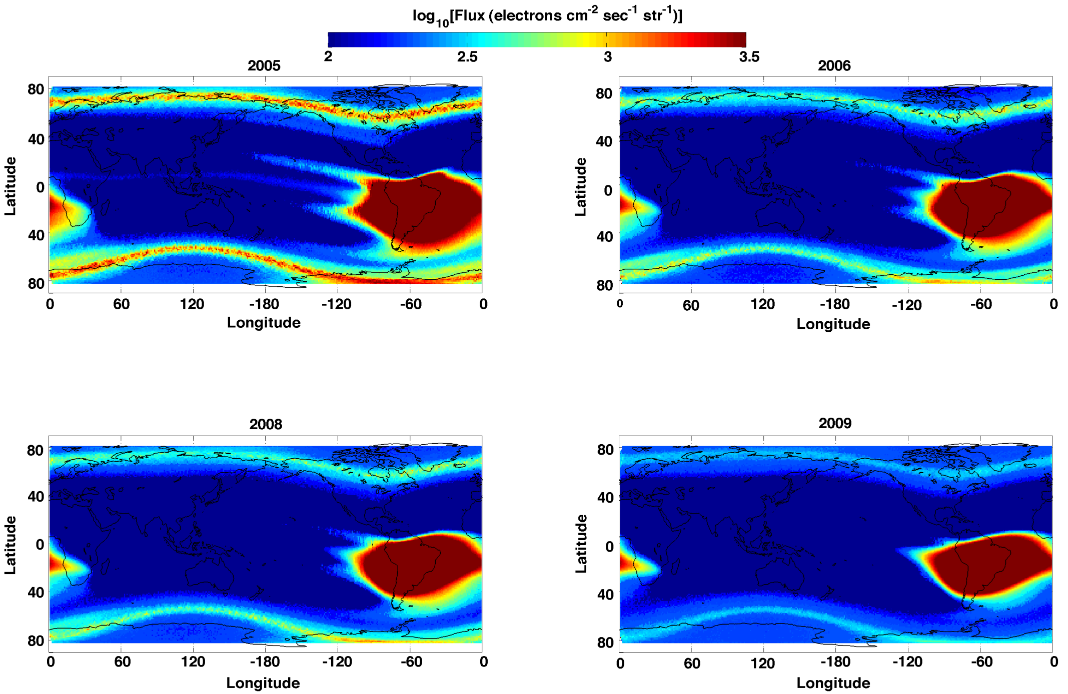

Fig. 1. World maps showing medians of > 30 keV precipitating electrons observed by the 0° directed MEPED–telescopes onboard POES in 2005, 2006, 2008 and 2009.

ACPD
13, 19895–19919, 2013

Electron precipitation and spatial OH variations

M. E. Andersson et al.

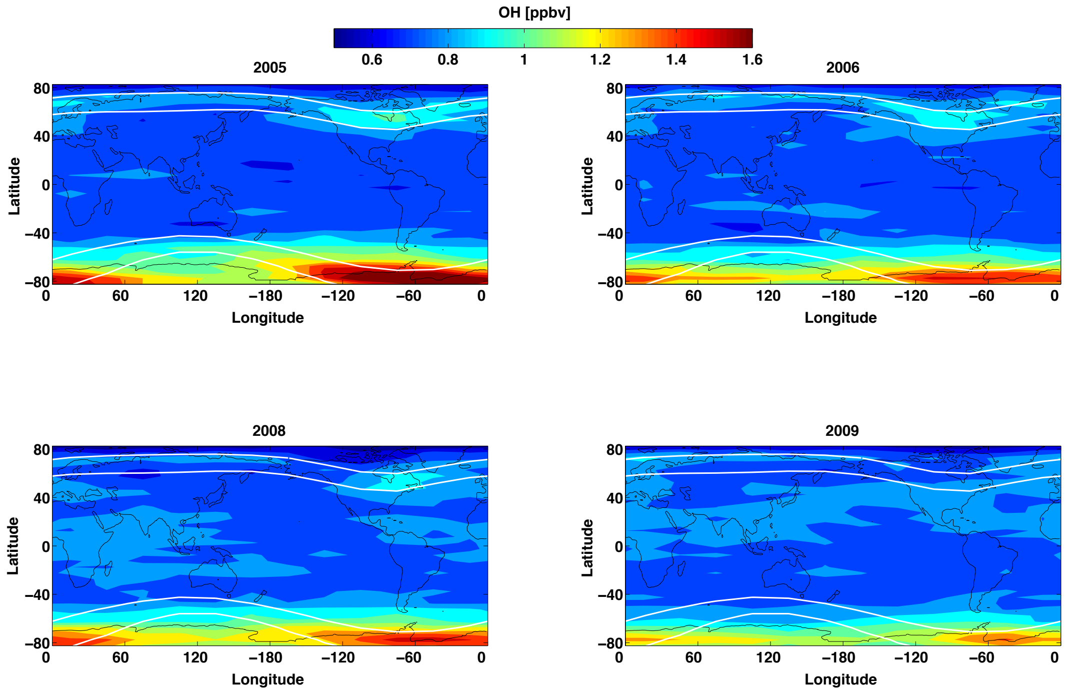

Fig. 2. World maps showing medians of nighttime OH in 2005, 2006, 2008 and 2009 averaged between 70–78 km. Median values were calculated for each 5 (latitude) × 30 (longitude) degree bins between latitudes 82° N to 82° S and longitudes 180° W to 180° E. Approximate geomagnetic latitudes 55–72° N/S are indicated by superimposed white lines.

ACPD
13, 19895–19919, 2013

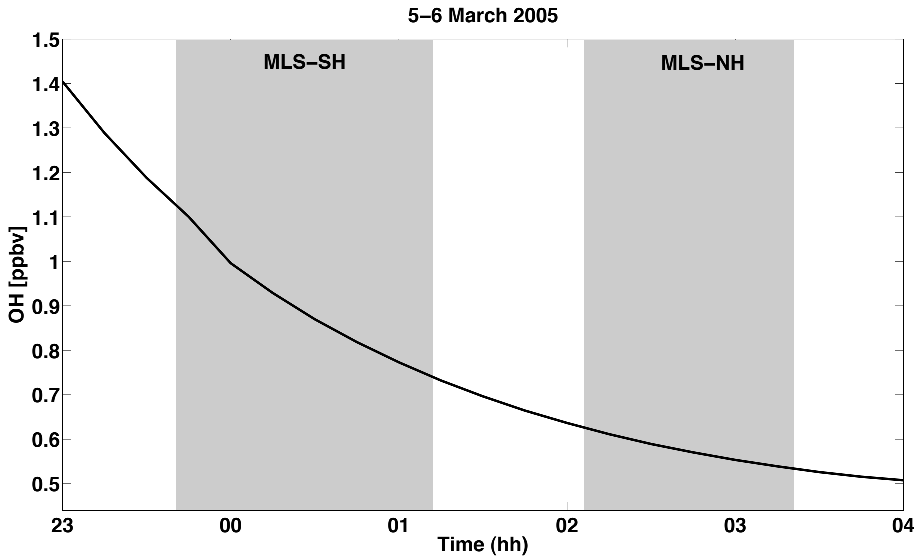

Fig. 3. OH mixing ratio from SIC model for 5–6 March 2005 averaged between 70–78 km. Approximate LST times of MLS measurements for NH nad SH are indicated by grey areas.

ACPD
13, 19895–19919, 2013

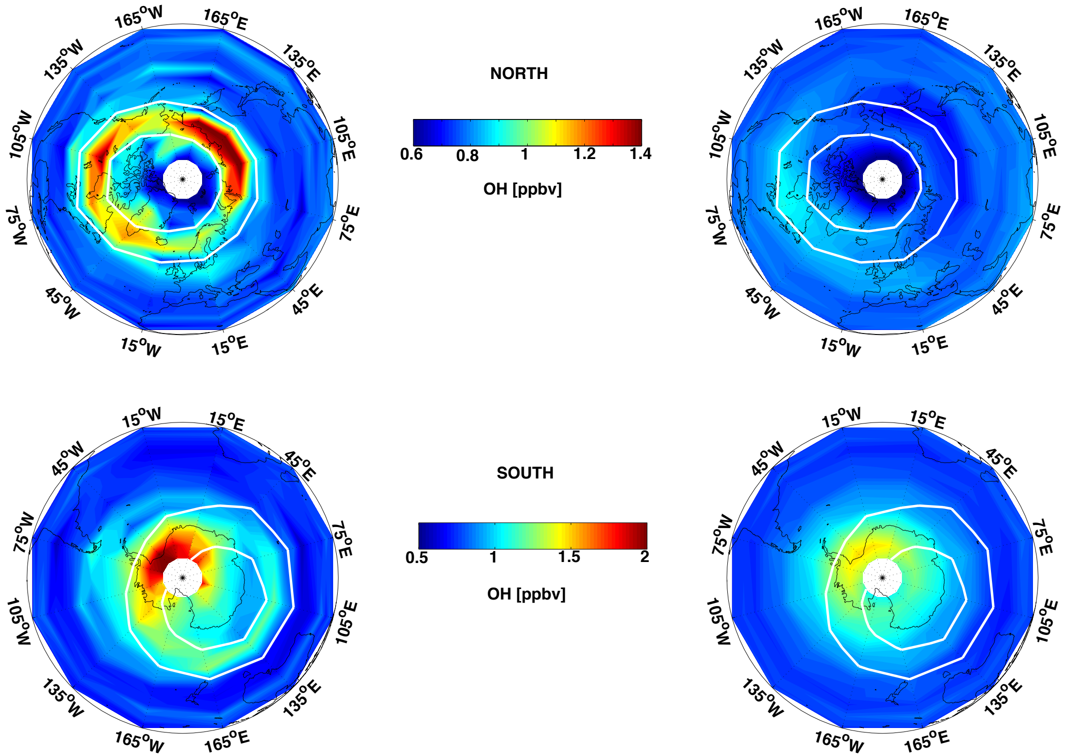

Fig. 4. Top panels: spatial distribution of OH medians in the NH calculated for the days with: (1) ECR > 100 counts s^{-1} (left panel) and (2) ECR < 5 counts s^{-1} (right panel) for the time period January 2005–December 2009 and altitude range 70–78 km. Bottom panels as top panels for the SH. Median values were calculated for each 5 (latitude) × 30 (longitude) degree bin between latitudes 82° N to 82° S and longitudes 180° W to 180° E. Approximate geomagnetic latitudes 55–72° N/S are indicated by superimposed white lines.

ACPD
13, 19895–19919, 2013

ACPD
13, 19895–19919, 2013

Electron precipitation and spatial OH variations

M. E. Andersson et al.

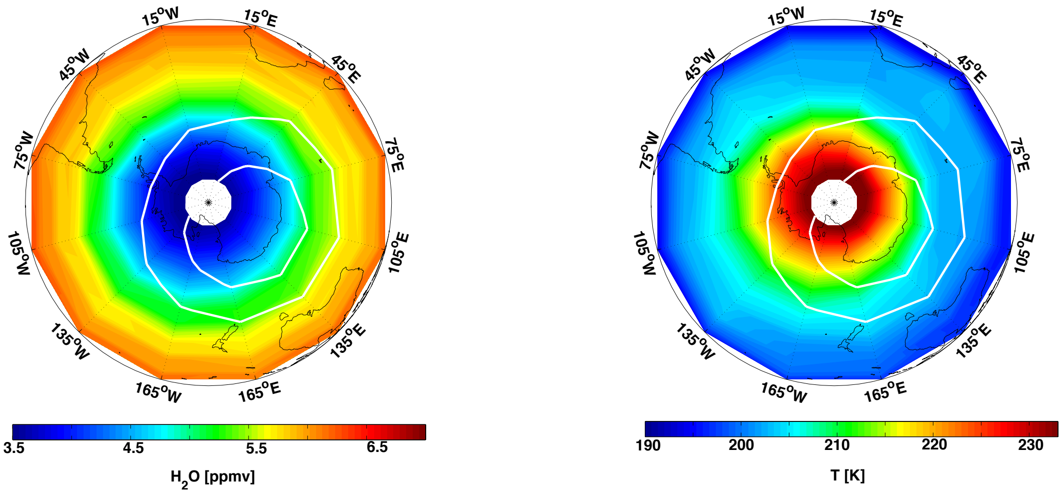

Fig. 5. Spatial distribution of H_2O (left panel) and temperature (right panel) medians during low EEP period (case II) averaged between 70–76 km. Median values were calculated for each 5 (latitude) × 30 (longitude) degree bins between latitudes 82° N to 82° S and longitudes 180° W to 180° E. Approximate geomagnetic latitudes 55–72° N/S are indicated by superimposed white lines.

ACPD
13, 19895–19919, 2013

Electron precipitation and spatial OH variations

M. E. Andersson et al.

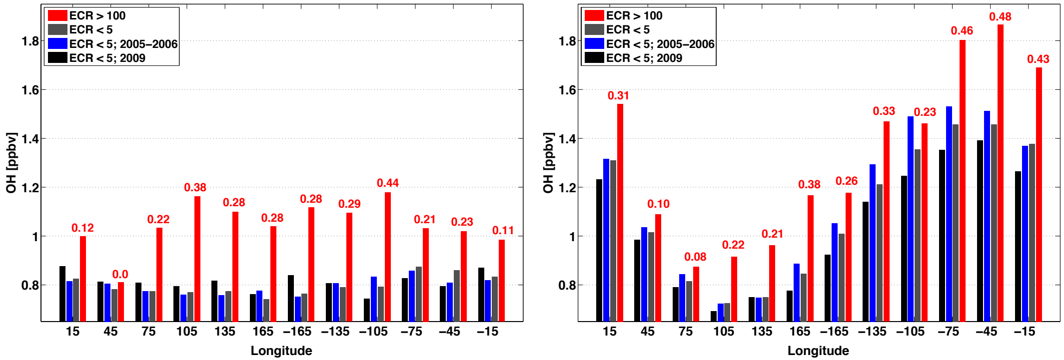

Fig. 6. Longitudinal variations of OH medians at geomagnetic latitudes 55–72° N (left panel) and 55–72° S (right panel) and altitudes between 70–78 km for 4 selected cases (see description in the text). Numbers indicate the absolute (ppbv, red) difference between OH during high EEP (case I) and the OH during the low geomagnetic activity (case IV).

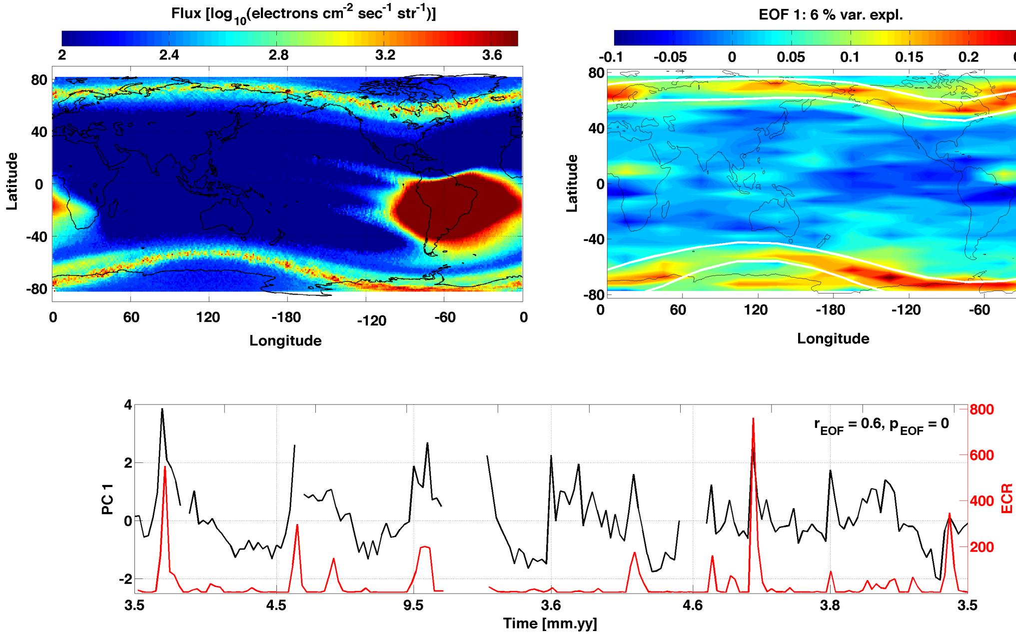

Fig. 7. Top left panel: world maps showing medians of > 30 keV precipitating electrons observed by the 0° directed MEPED–telescopes onboard POES for 6 selected month (see description in the text). Top right panel: first EOF mode as a function of latitude and longitude for selected months between January 2005–December 2009. Numbers in percent indicate variance represented by each mode to the total variance. Bottom panel: the PC (black lines) of the first EOF mode. Red line represents the daily mean electron count rates. Approximate geomagnetic latitudes 55–72° N/S are indicated by superimposed white lines.

ACPD
13, 19895–19919, 2013

Electron precipitation and spatial OH variations

M. E. Andersson et al.